High frequency ultrasound imaging and simulations of sea urchin oocytes

Eric M. Strohm, Lauren A. Wirtzfeld, Gregory J. Czarnota, and Michael C. Kolios

Citation: The Journal of the Acoustical Society of America **142**, 268 (2017);
View online: https://doi.org/10.1121/1.4993594
View Table of Contents: http://asa.scitation.org/toc/jas/142/1
Published by the Acoustical Society of America

High frequency ultrasound imaging and simulations of sea urchin oocytes

Eric M. Strohm and Lauren A. Wirtzfeld
Department of Physics, Ryerson University, 350 Victoria Street, Toronto, Ontario M5B 2K3, Canada

Gregory J. Czarnota
Senior Scientist and Director, Odette Cancer Research Program, Sunnybrook Research Institute, 2075 Bayview Avenue, Toronto, Ontario M4N 3M5, Canada

Michael C. Kolios[a)]
Department of Physics, Ryerson University, 350 Victoria Street, Toronto, Ontario M5B 2K3, Canada

(Received 25 January 2017; revised 20 June 2017; accepted 25 June 2017; published online 19 July 2017)

High frequency ultrasound backscatter signals from sea urchin oocytes were measured using a 40 MHz transducer and compared to numerical simulations. The Faran scattering model was used to calculate the ultrasound scattered from single oocytes in suspension. The urchin oocytes are non-nucleated with uniform size and biomechanical properties; the backscatter from each cell is similar and easy to simulate, unlike typical nucleated mammalian cells. The time domain signal measured from single oocytes in suspension showed two distinct peaks, and the power spectrum was periodic with minima spaced approximately 10 MHz apart. Good agreement to the Faran scattering model was observed. Measurements from tightly packed oocyte cell pellets showed similar periodic features in the power spectra, which was a result of the uniform size and consistent biomechanical properties of the cells. Numerical simulations that calculated the ultrasound scattered from individual oocytes within a three dimensional volume showed good agreement to the measured signals and B-scan images. A cepstral analysis of the signal was used to calculate the size of the cells, which was 78.7 μm (measured) and 81.4 μm (simulated). This work supports the single scattering approximation, where ultrasound is discretely scattered from single cells within a bulk homogeneous sample, and that multiple scattering has a negligible effect. This technique can be applied towards understanding the complex scattering behaviour from heterogeneous tissues. © *2017 Acoustical Society of America*. [http://dx.doi.org/10.1121/1.4993594]

[CC] Pages: 268–275

I. INTRODUCTION

The scattering of sound waves from cells and tissues depends strongly on the biomechanical properties of tissues, which itself depends on the type of tissues examined.[1] A quantitative analysis of the scattered ultrasound signals can be used to assess tissue types and their health.[2–4] Quantitative ultrasound (QUS) techniques have been applied towards detecting apoptosis *in vitro* and *in vivo*,[5–11] characterizing tissues using the mean scatterer diameter and spacing,[12–21] analysis of blood,[22–26] calculating cell and microparticle physical properties,[27–30] detecting cancer *ex vivo*,[31–34] and characterizing bone structure.[35–37]

Numerous experimental studies have been performed examining the ultrasound scattering from tissues, and how it can be used to infer properties of the tissues, however the scattering phenomena is not well understood. Changes in the ultrasound signals have been hypothesized to be due to variations in the pseudorandom spatial arrangement, cellular biomechanical properties, and/or nuclear/cell size and shape.[38–41] Early computer simulations examined the ultrasound scattered from sub-resolution scatterers within a tissue volume.[42–45] These simulations convolved the transducer impulse response with the scatterers in the medium, and demonstrated that the transducer beam properties such as the lateral resolution and transducer geometry influenced the speckle pattern in the generated B-scans. Later simulation techniques describe biomechanical inhomogeneities as distributions through the tissue samples, and calculated the backscatter based on Rayleigh statistics, K-distribution,[46–49] or Nakagami distribution.[50–52] Other models include the Gaussian form factor model which assumes a random collection of spherical scatterers to calculate the ultrasound backscatter,[12,53–55] and the structure factor model which accounts for correlations between cell positions in the tissue.[56–59]

The aforementioned modeling techniques use estimations or distributions to calculate the ultrasound from a collection of cells. Approximations can result in diverging solutions when used inappropriately within incorrect ka ranges.[60,61] Arguably a more accurate technique is to calculate and sum the ultrasound scattered from each discrete scatterer, but this is computationally intensive and quickly scales with the number of scatterers, limiting the volume that can be simulated.

Each cell is a viscoelastic mixture of fluids, proteins and organelles which behaves as a poroelastic material when under load;[62–64] the cells can be considered homogeneous on the length scales used in these ultrasound studies. Discrete modeling techniques include simulating the cell or nucleus as the dominant scatterer[57,60,65–70] or as two concentric spheres.[18,55,71,72] Due to the computational time and

[a)]Electronic mail: mkolios@ryerson.ca

complexity, these models are generally restricted to two dimensional (2D) areas or small volumes only. Our previous work in measuring ultrasound scattered from single cells showed that modeling the cell as a homogeneous Newtonian inviscid fluid filled sphere suspended in a Newtonian inviscid fluid is a valid approximation, with good agreement to theoretical predictions.[70,73] Our model calculates the ultrasound scattered from each individual cell within a three dimensional (3D) volume, and then applies weights to the signal from each cell depending on its location within the limited field of view (FOV). The superposition of signals from each cell within the transducer FOV can be calculated, creating a matrix of ultrasound signals as a function of measurement location.

Theoretical scattering of sound waves from homogeneous spheres dates back to the 1950s.[74–83] For an incident plane wave propagating in a Newtonian inviscid fluid and incident on an elastic spherical scatterer, the analytical solution for the far-field pressure amplitude of the scattered ultrasound wave P_s in the frequency domain is

$$P_s(r,\theta,f) = \frac{P_0}{akr}\sum_{n=0}^{\infty}\left[(-i)^n(2n+1)\sin\eta_n \times \exp(-i\eta_n)P_n(\cos\theta)\right]\exp(-ikr), \quad (1)$$

where P_0 is the initial ultrasound pressure, r is the distance to the observation point, n is the order of the scattered wave, P_n is the nth order Legendre function, a is the radius, $k = 2\pi f/c$, θ is the scattering angle (where 180° denotes a backscattered wave) and η is the phase-shift angle as defined in[76,77] which itself is a function of ka of the cell and the coupling fluid, and also the Poisson ratio of the cell. This equation was developed by Faran in 1951 (Ref. 76) and then refined by Hickling in 1962 (Ref. 77); it accounts for shear and compressional waves in the elastic scatterers. This solution was shown to be identical to the Anderson fluid filled spherical model[74] when shear waves can be neglected (i.e., the Poisson ratio was 0.4993 or higher).[60] Multiple scattering was ignored as it has a negligible contribution to the overall signal for weak scatterers.

Sea urchin oocytes are homogeneous with a narrow size distribution. They are composed mostly of fluids, protein and egg yolk,[84] with a $ka = 7.1$ at 40 MHz, and are ideal for studies that use a discrete ultrasound scatterer simulation technique. The ultrasound scattered from single oocytes and close-packed cell pellets were examined to help understand the ultrasound scattering from cell aggregates. Good agreement between the measured and simulated signals was observed, validating the numerical simulations and supporting the single scattering approximation theory. This model can be used for studying the ultrasound scattered from more complex scenarios such as heterogeneous tissues, where the scattering phenomenon is not well understood.

II. METHOD

A. Sea urchin oocyte preparation

Purple sea urchin oocytes *strongylocentrotus purpuratus* were prepared in an artificial hypertonic salt water solution containing 0.5 M KCl. Live female sea urchins were placed in the salt solution, shedding oocytes into the water which were collected for analysis. The average diameter of the cells was 85 μm [Fig. 1(A)]. Oocytes suspended in a 0.5 M KCl solution were used for the single cell measurements. The ultrasound transducer was immersed into the fluid, which was gently stirred prior to recording the signals. Cell pellets were made by centrifuging the oocyte cells in an 8 mm diameter container at approximately 200 g for 10 min, which created a close-packed structure of cells to mimic normal tissue. The cell pellet was measured with ultrasound in degassed PBS at room temperature [Fig. 1(B)].

B. Ultrasound measurements

Measurements were performed using a Visualsonics VS40B Ultrasound Scanning System using a 40 MHz transducer (Visualsonics Inc., Toronto, Canada). The transducer had a focal length of 9 mm, f# of 3.0, and a −6 dB bandwidth of 90% as measured from the reflection from a quartz plate. All data were sampled at 500 MS/s and analyzed using Matlab. The normalized power spectrum P was calculated using equation

$$P = 10\log_{10}\left|\frac{P_m(x,y,z,f)^2}{P_{\mathrm{ref}}(f)^2}\right|, \quad (2)$$

where P_m is the power spectrum of the measured time domain signal and P_{ref} is the reference spectrum measured from a quartz substrate.[68] The power cepstrum was calculated using the inverse Fourier transform of the logarithm of the spectrum.[37,85–87]

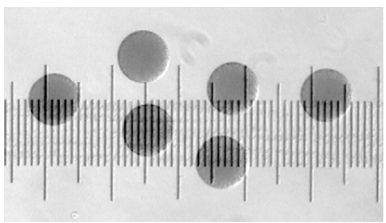

(A)

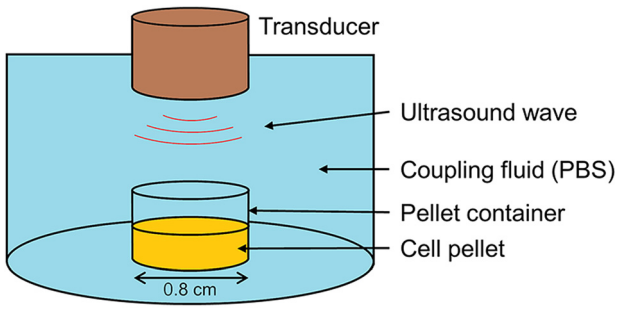

(B)

FIG. 1. (Color online) (A) Optical image of the sea urchin oocytes superimposed over a scale bar. The major division is 100 μm. (B) Schematic showing the experimental setup, with the transducer above the cell pellet.

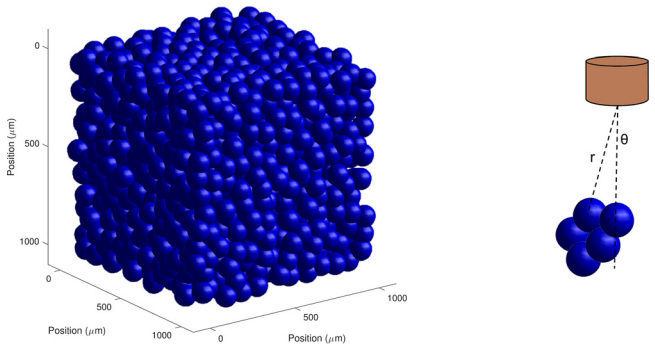

FIG. 2. (Color online) (A) A pictorial representation of the close-packed nature of the cells generated for the simulations. (B) Calculation of the ultrasound signal from each cell as a function of distance r and angle θ.

C. Numerical simulations

1. Spatial organization

A $5 \times 5 \times 1\,\text{mm}^3$ volume of cells was created by using an algorithm to randomly place cells within the volume. The algorithm sequentially placed cells such that a newly placed cell was at least a minimum distance from its closest neighbours. For a close-packed structure of non-deformable non-overlapping spheres, the volume packing ratio is a maximum of 0.74 for a periodic face-centered cubic (FCC) structure,[88] and drops to the 0.6 range for randomly packed spheres.[89] To achieve a realistic tissue packing ratio of 0.75–0.90,[90] the spheres were allowed to overlap slightly. Using a minimum center−center distance of 55 μm, a volume packing ratio of 0.78 was achieved using 60703 cells of 85 μm diameter in a $5 \times 5 \times 1$ mm volume (Fig. 2).

2. Ultrasound scattering model

Using 40 MHz ultrasound with a cell diameter of 85 μm, ka = 7.1. Calculations using Rayleigh scattering equations can be used when ka $\ll$ 1; as ka increases towards 1, the scatterer shape and scattering angle becomes important and Rayleigh scattering breaks down.[91–93] Equation (1), known as the Faran model, can be used to calculate the exact solution of the scattered ultrasound over a wide range wide of ka values, with the assumption that the scatterer is spherical and homogeneous.[76,77] The ultrasound scattered from a region of interest within the cell pellet was simulated by calculating the ultrasound scattered from each individual cell using the Faran scattering model and then summing the scattered waves from each individual cell. Multiple scattering was ignored, as the backscattered signal amplitude from a single cell was 0.3% of the signal amplitude measured from a quartz plate; thus, multiple scattering would have a negligible effect on the overall measured signal.

The input parameters for the Faran model were $v_f = 1480$ m/s (for PBS) or 1525 m/s (for 0.5 M KCl saltwater[94]), $v_s = 1573$ m/s,[69] $\rho_f = 1000\,\text{kg/m}^3$, $\rho_s = 1198\,\text{kg/m}^3$,[69] and a Poisson ratio of 0.499, where the subscript f denotes the coupling fluid, and the subscript s denotes the spherical cell.

The transducer was positioned above the cell pellet as shown in Fig. 2, and the ultrasound signals from cells as a function of distance r and angle θ was calculated. The transducer position was moved along the x axis, and the calculations repeated. The ultrasound signal p measured with the transducer focal spot at a location (x, y, z) was

$$p(x,y,z,t) = \sum_n p_s(r,\theta,f) W_{\text{lateral}}(x_n) W_{\text{lateral}}(y_n) W_{\text{axial}}(z_n), \tag{3}$$

where $p_s(r, \theta, f)$ is the time domain signal from each cell [Eq. (1)], and W is a weight that accounts for the decrease in signal for cells outside of the transducer FOV. The 40 MHz transducer used in the measurements had a lateral resolution of 115 μm and a depth of field of 2.5 mm. A Gaussian distribution with $\mu = 0$ and $\sigma = 50$ for the x and y coordinates, and $\mu = 0$ and $\sigma = 1075$ for the z coordinate were used for the weights. The angle θ and distance r was calculated from the lateral and axial coordinates of the cell location relative to the transducer, and are required components of the Faran solution.

The algorithm was optimized to use a lookup table instead of calculating the Faran solution for each cell. A lookup table that contained the Faran solution for all angles θ was created and saved over a frequency range of 0–400 MHz. The algorithm stepped over every cell in the volume and if the cell was outside of the transducer FOV [i.e., the product of the axial and lateral weights in Eq. (3) was < 0.001], then the signal from that cell was set to zero and the algorithm moved onto the next cell. For all cells within the transducer FOV, the frequency domain Faran solution as a function of r and θ was found using the lookup table. The inverse Fourier Transform was calculated for the signal from each cell, then the FOV weights applied. A bandpass filter of 20–55 MHz applied to account for the limited bandwidth of the VS-40B transducer, and then all the

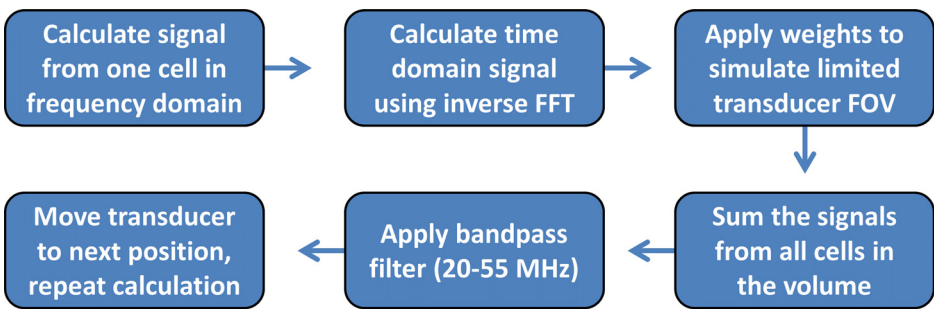

FIG. 3. (Color online) A block diagram describing the numerical simulation algorithm.

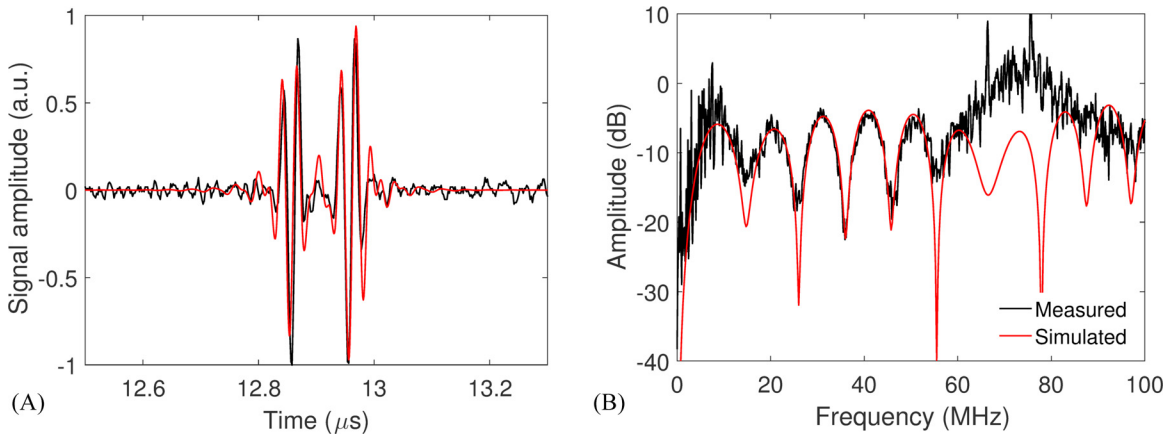

FIG. 4. (Color online) (A) A representative time domain signal measured (black) and simulated (red) from a single oocyte using 40 MHz. (B) The spectrum of the measured (black) and simulated (red) oocyte.

signals were summed to give the collective signal from all scatterers at that transducer position. The transducer was moved along the x axis using the predefined step size, and then the signals from the cells within the new FOV were calculated using the same procedure. This process was repeated along the x axis from 0 to 5 mm in steps in 10 μm. The process is illustrated using a block diagram in Fig. 3.

B-scan images were created by converting the A-lines at each transducer position to a grayscale intensity with the maximum signal level white, and the lowest black. Simulated images were created by log compressing the signal envelope and adjusting the dynamic range to match the measured images.

III. RESULTS

A. Single cells

Single cells in a suspension of saltwater were measured and compared to theoretical predictions. Figure 4 shows a representative measured time domain signal and spectrum for a single oocyte. Optical microscopy confirmed that the cells were not aggregating, and ultrasound imaging would reveal the presence of more than one cell within the FOV. The time domain signal showed two peaks separated in time, which resemble echoes from the front and back of the oocyte.[69] The spectrum for the oocytes measured in suspension was calculated from the time domain signal, while the theoretical spectrum was solved using Eq. (1) and the time domain signal calculated from the inverse Fourier transform. A bandpass filter of 25–55 MHz was applied to the theoretical time domain signal for direct comparison to the measured signal. Good agreement in the shape and features of the time domain signals and their spectra were observed.

A collection of six oocytes in suspension was simulated by randomly positioning the cells in a 2D spatial arrangement, then a B-scan created by calculating the ultrasound signal at points along the x axis using 10 μm steps. A bandpass filter of 25–55 MHz was then applied. A limited FOV using a weighted Gaussian resolution profile as described in the methods to ensure that the six cells were sufficiently separated and that the ultrasound signals were independent. Figure 5 shows a measured B-scan from the oocytes in suspension compared to the simulated B-scan. In both images, the lateral spread of the signal was approximately 250 μm, and the time between the two scattered signals of each cell were 100 ns, or 78.65 μm when converted to distance ($d = [1/2]$*v*t) using a sound speed of 1573 m/s.

B. Cell pellets

The oocyte cell pellets were imaged using a 40 MHz transducer, the resulting B-scan is shown in Fig. 6. A simulated B-scan image created from a 3D spatial arrangement of cells as described in the methods section is also shown in Fig. 6. Representative A-scan signals are shown in Fig. 7. The measured pellet shows an irregular pellet-liquid interface at the top due to inhomogeneities within the pellet, where single oocytes can be observed above the pellet in some cases. The simulated pellet was modeled with sharp

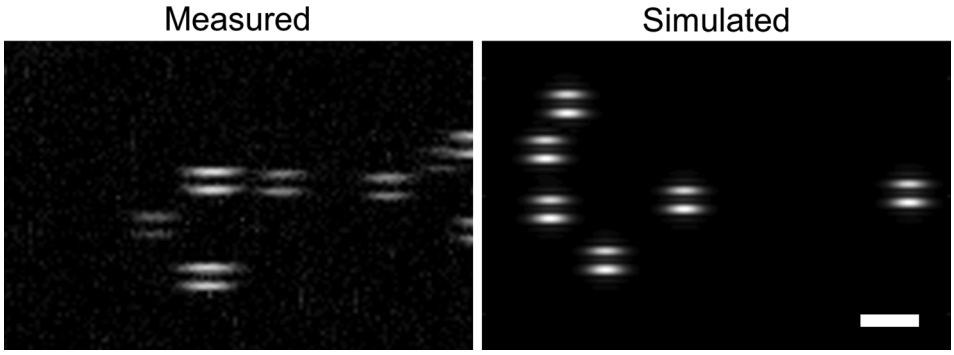

FIG. 5. B-scans of single oocytes in suspension at 40 MHz: experimental (left) and simulated (right). The scale bar is 250 μm.

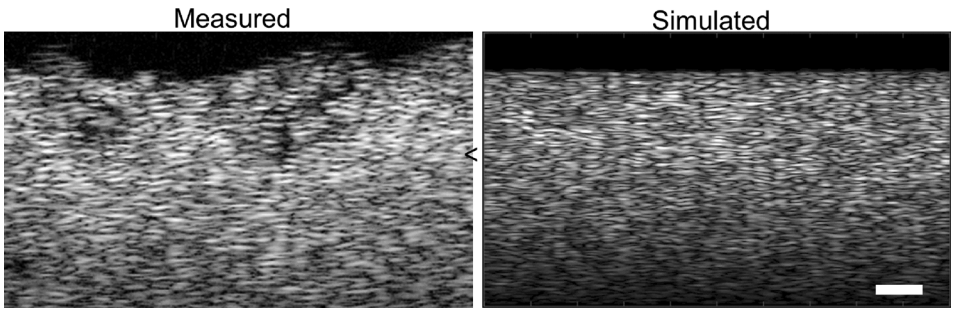

FIG. 6. B-scan images created from oocyte pellets using 40 MHz ultrasound: experimental (left) and simulated (right) B-scans. The scale bar is 250 μm.

borders, so this behavior was not observed. The power cepstrum was calculated for both the measured and simulated cell pellet in the z-axis direction (into the pellet). Rahmonics were located at 50.03 ns (measured data) and 51.75 ns (simulated data). The quefrequency has units of seconds, and was converted to distance using the relation $d = v^*t$, where the sound speed of the cells, 1573 m/s was used. Using this conversion, the cell pellet had a peak at 78.7 μm, while the simulated pellet showed a peak at 81.4 μm (Fig. 9).

IV. DISCUSSION

A numerical simulation technique that calculates the ultrasound scattered from every cell within a 3D volume was developed to help understand the contribution of single scatterers on the measured ultrasound signal from bulk tissues. Modern computers are now fast enough to calculate the signal from all scatterers in a volume within a reasonable amount of time. Using a lookup table, the simulation time for 60703 cells in a $5 \times 5 \times 1$ mm volume using a standard Intel i7 desktop PC was about 5 min. This can easily scale to larger volumes and smaller scatterers.

For the single cell measurements, there was good agreement between the measured and simulated signals in both the time and frequency domains using a cell diameter of 79 μm and a sound speed and density of 1573 m/s and 1198 kg/m^3, respectively. Excellent agreement between measured and simulated in both the frequency and time domain were observed (Fig. 4), as indicated by the overlap of the two signals. A comparison between theoretical and measured signals of single urchin oocytes using frequencies at 20, 40, and 55 MHz was previously demonstrated by Falou *et al.*[69] Using the Anderson scattering model,[74] they found that a cell diameter of 75 μm with a sound speed and density of 1573 m/s and 1198 kg/m^3, respectively, fit well with measured signals. The slight difference in the calculated cell diameter between their results and ours may be due to differences in the experimental conditions/procedures, cell preparations, and the model used (Faran vs Anderson). Figure 5 shows good agreement in the lateral spread and the axial signal intensity between measured and theoretical B-scans of several oocytes.

Modeling the ultrasound scattering from single oocytes validated the model, which could then be applied to measurements from a tightly packed 3D structure of cells. The measured and simulated a-scans from packed oocytes are shown in Fig. 6. The transducer focus was approximately 1 mm below the surface of the cell pellet, resulting in a signal amplitude maximum at approximately 11 μs. Attenuation was not modeled as its contribution would be significantly less than the contributions of the focal gain/loss at the frequencies used. The A-scans were used to recreate the measured and simulated B-scans as shown in Fig. 7. The measured region of interest (ROI) was 8×8 cm^2, while the simulated ROI was 5×5 cm^2. Both regions were cropped to a 2.5×1.5 cm^2 area for better evaluation. The surface of the measured cell pellet was uneven and some voids were visible within the pellet, which was likely due to some disassociation during the measurement. Otherwise, the measured and simulated B-scans showed similar variations in intensity due to the pseudo random packing nature of the cells.

A quantitative analysis of the cell pellet RF data was used to extract information about the cells. The power

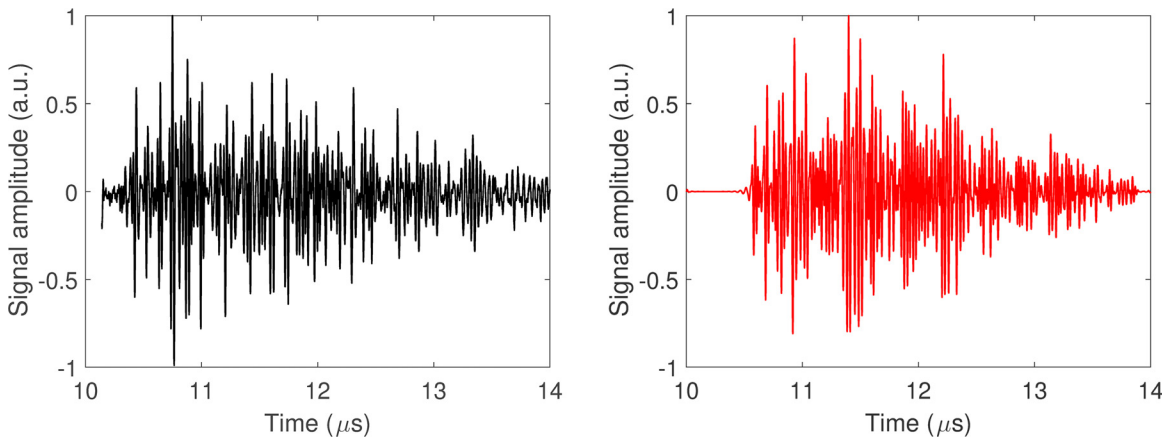

FIG. 7. (Color online) Representative time domain backscatter signal from oocyte pellets using 40 MHz ultrasound: experimental (left) and simulated (right).

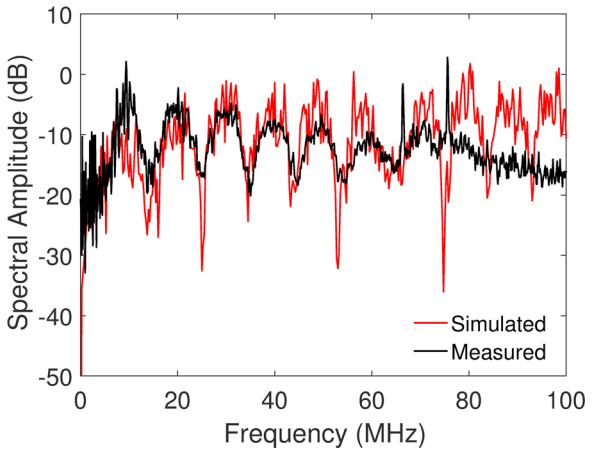

FIG. 8. (Color online) The power spectra of 30 individual signals were calculated and then averaged together for both the experimental (black) and simulated (red). Good agreement in the location of the spectral minima and maxima were observed.

spectra from 30 individual RF lines were calculated, and then averaged (Fig. 8). A periodically varying spectral pattern was observed for both the measured and simulated data; this pattern was not clearly visible in the unaveraged spectra. Compared to the single cell measurements (Fig. 4), there was good agreement in the location of the minima and maxima throughout the bandwidth of the spectra (20–60 MHz). This supports the single scattering approximation, where scattering from closed packed cells occurs from each individual cells within the FOV, and that multiple scattering has a negligible effect.

The cepstrum is useful for detecting periodicity in the spectrum. From Figs. 4 and 8, it is evident that there is a periodic pattern in the spectrum. Using the power cepstrum, the period of this spectral pattern was 50.0 ns (measured data) and 51.8 ns (simulated data). When converted to spatial distance using d = v*t, using v = 1573 m/s, this corresponds to a distance of 78.7 μm (measured data) and 81.4 μm (simulated data) as shown in Fig. 9. For the measured data, the cepstrum calculation of 78.7 μm matched the size estimation using the measured peak−peak time domain signal of a single cell (78.7 μm, Sec. III A). For the simulated data, the cepstrum calculation of 81.4 μm was slightly lower than the urchin diameter used in the simulations 85 μm. The 85 μm diameter was used in the simulations as it gave the best match in the location of the spectral minima and maxima as shown in Fig. 8. Thus, the cepstrum can be use to estimate the size of the cells within a bulk tissue structure.

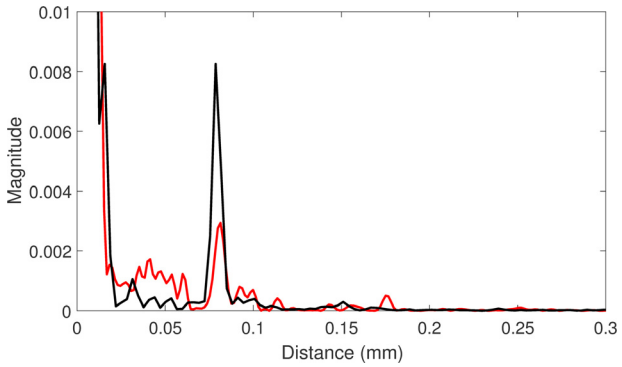

FIG. 9. (Color online) The cepstra derived from the backscatter signal from oocyte pellets: experimental (black) and simulated (red). A peak was observed at 78.7 μm (experimental) and 81.4 μm (simulated).

The technique developed in this study can rapidly simulate the ultrasound scattering from bulk tissues by calculating the signals from every individual scatterer within bulk tissues. Larger volumes and smaller cells can be examined, as well as variations in size distributions, cell structures and biomechanical properties, and applied to photoacoustic imaging applications.[95,96] A 3D environment more accurately simulates the scattering behaviour compared to 2D simulations typically used in ultrasound. For future work, simulations of heterogeneous tissues will be performed, where the cell size distributions and cell spatial organizations are mapped using histological samples of cell pellets and tissues. This will help understand how size and structure affect ultrasound scattering. The ultrasound scattered from tissues that are undergoing apoptosis increases significantly compared to healthy tissue, however, this process is not fully understood. An iterative process of adjusting the cell sizes, distributions, and biomechanical properties will be performed to examine how these changes affect the ultrasound scattering.

V. CONCLUSIONS

A technique to numerically simulate the ultrasound scattered from individual cells within a 3D close-packed structure of cells was developed and compared to measurements of sea urchin oocytes using 40 MHz ultrasound. Excellent agreement in the measured A-scans and recreated B-scan images was observed from both single cells, as well as close-packed cell pellets which simulated a tissue environment. The results support the single scattering approximation, where scattering occurs from individual cells and multiple scattering can be neglected. The simulation technique is fast and easy to implement, with applications in calculating the ultrasound scattered from heterogeneous tissues composed of varying cell sizes and types.

ACKNOWLEDGMENTS

The authors would like to thank Zenon Harley and Homayoun Vaziri for their expertise and guidance and providing the sea urchin oocytes, Ralph Baddour and Noel Nathanael (University of Toronto) for acquiring data, Arthur Worthington (Ryerson University) for technical assistance, and Elizabeth Berndl (Ryerson University) for assistance with manuscript preparation. This research was supported by the Terry Fox Foundation, Canadian Foundation for Innovation, the Ontario Innovation Trust, Canadian Health Institutes for Health Research, and the Natural Sciences and Engineering Research Council of Canada.

[1]F. A. Duck, *Physical Properties of Tissue: A Comprehensive Reference Book* (Academic, San Diego, 1990), 336 pp.
[2]K. K. Shung and G. A. Thieme, *Ultrasonic Scattering in Biological Tissues* (CRC Press, Ann Arbor, MI, 1992), 520 pp.
[3]J. Mamou and M. L. Oelze, eds., *Quantitative Ultrasound in Soft Tissues* (Springer, Dordrecht, 2013), 444 pp.

[4]M. L. Oelze and J. Mamou, "Review of quantitative ultrasound: Envelope statistics and backscatter coefficient imaging and contributions to diagnostic ultrasound," IEEE Trans. Ultrason., Ferroelectr., Frequency Control **63**, 336–351 (2016).
[5]G. J. Czarnota, M. C. Kolios, J. Abraham, M. Portnoy, F. P. Ottensmeyer, J. W. Hunt, and M. D. Sherar, "Ultrasound imaging of apoptosis: High-resolution non-invasive monitoring of programmed cell death *in vitro*, *in situ* and *in vivo*," Br. J. Cancer **81**, 520–527 (1999).
[6]A. Sadeghi-Naini, O. Falou, J. M. Hudson, C. Bailey, P. N. Burns, M. J. Yaffe, G. J. Stanisz, M. C. Kolios, and G. J. Czarnota, "Imaging innovations for cancer therapy response monitoring," Imag. Med. **4**, 311–327 (2012).
[7]A. Sadeghi-Naini, N. Papanicolau, O. Falou, J. Zubovits, R. Dent, S. Verma, M. Trudeau, J. F. Boileau, J. F. Boileau, J. Spayne, S. Iradji, E. Sofroni, J. Lee, S. Lemon-Wong, M. Yaffe, M. C. Kolios, and G. J. Czarnota, "Quantitative ultrasound evaluation of tumor cell death response in locally advanced breast cancer patients receiving chemotherapy," Clin. Cancer Res. **19**, 2163–2174 (2013).
[8]A. Sadeghi-Naini, O. Falou, H. Tadayyon, A. Al-Mahrouki, W. Tran, N. Papanicolau, M. C. Kolios, and G. J. Czarnota, "Conventional frequency ultrasonic biomarkers of cancer treatment response *in vivo*," Transl. Oncol. **6**, 234–243 (2013).
[9]A. Sadeghi-Naini, L. Sannachi, K. Pritchard, M. Trudeau, S. Gandhi, F. C. Wright, J. Zubovits, M. J. Yaffe, M. C. Kolios, and G. J. Czarnota, "Early prediction of therapy responses and outcomes in breast cancer patients using quantitative ultrasound spectral texture," Oncotarget **5**, 3497–3511 (2014).
[10]H. Tadayyon, A. Sadeghi-Naini, and G. J. Czarnota, "Noninvasive characterization of locally advanced breast cancer using textural analysis of quantitative ultrasound parametric images," Transl. Oncol. **7**, 759–767 (2014).
[11]L. Sannachi, H. Tadayyon, A. Sadeghi-Naini, W. Tran, S. Gandhi, F. Wright, M. Oelze, and G. Czarnota, "Non-invasive evaluation of breast cancer response to chemotherapy using quantitative ultrasonic backscatter parameters," Med. Image Anal. **20**, 224–236 (2015).
[12]M. L. Oelze, J. F. Zachary, and W. D. O'Brien, "Characterization of tissue microstructure using ultrasonic backscatter: Theory and technique for optimization using a Gaussian form factor," J. Acoust. Soc. Am. **112**, 1202–1211 (2002).
[13]M. L. Oelze and W. D. O'Brien, "Method of improved scatterer size estimation and application to parametric imaging using ultrasound," J. Acoust. Soc. Am. **112**, 3053–3063 (2002).
[14]J. Mamou, M. L. Oelze, W. D. O'Brien, and J. F. Zachary, "Identifying ultrasonic scattering sites from three-dimensional impedance maps," J. Acoust. Soc. Am. **117**, 413–423 (2005).
[15]R. Lavarello and M. Oelze, "Quantitative ultrasound estimates from populations of scatterers with continuous size distributions," IEEE Trans. Ultrason., Ferroelectr. Frequency Control **58**, 744–753 (2011).
[16]A. Han and W. O'Brien, "Structure function for high-concentration biophantoms of polydisperse scatterer sizes," IEEE Trans. Ultrason., Ferroelectr., Frequency Control **62**, 303–318 (2015).
[17]L. X. Yao, J. A. Zagzebski, and E. L. Madsen, "Backscatter coefficient measurements using a reference phantom to extract depth-dependent instrumentation factors," Ultrason. Imag. **12**, 58–70 (1990).
[18]M. Teisseire, A. Han, R. Abuhabsah, J. P. Blue, S. Sarwate, and W. D. O'Brien, "Ultrasonic backscatter coefficient quantitative estimates from Chinese hamster ovary cell pellet biophantoms," J. Acoust. Soc. Am. **128**, 3175–3180 (2010).
[19]E. J. Feleppa, A. Kalisz, J. B. Sokil-Melgar, F. L. Lizzi, T. Liu, A. L. Rosado, M. C. Shao, W. R. Fair, Y. Wang, M. S. Cookson, V. E. Reuter, and W. D. W. Heston, "Typing of prostate tissue by ultrasonic spectrum analysis," IEEE Trans. Ultrason., Ferroelectr. Frequency Control **43**, 609–619 (1996).
[20]E. J. Feleppa, J. Mamou, C. R. Porter, and J. Machi, "Quantitative ultrasound in cancer imaging," Semin. Oncol. **38**, 136–150 (2011).
[21]K. P. Mercado, M. Helguera, D. C. Hocking, and D. Dalecki, "Estimating cell concentration in three-dimensional engineered tissues using high frequency quantitative ultrasound," Ann. Biomed. Eng. **42**, 1292–1304 (2014).
[22]M. A. H. Weiser and R. E. Apfel, "Extension of acoustic levitation to include the study of micron-size particles in a more compressible host liquid," J. Acoust. Soc. Am. **71**, 1261–1268 (1982).
[23]K. K. Shung, R. A. Sigelmann, and J. M. Reid, "Scattering of ultrasound by blood," IEEE Trans. Biomed. Eng. **23**, 460–467 (1976).
[24]Y. W. Yuan and K. K. Shung, "Ultrasonic backscatter from flowing whole blood. I: Dependence on shear rate and hematocrit," J. Acoust. Soc. Am. **84**, 52–58 (1988).
[25]Y. W. Yuan and K. K. Shung, "Ultrasonic backscatter from flowing whole blood. II: Dependence on frequency and fibrinogen concentration," J. Acoust. Soc. Am. **84**, 1195–1200 (1988).
[26]G. Cloutier and Z. Qin, "Ultrasound backscattering from non-aggregating and aggregating erythrocytes—A review," Biorheology **34**, 443–470 (1997).
[27]R. Roy, "Quantitative particle characterization by scattered ultrasound," Ph.D. dissertation, Yale University, New Haven, CT, 1987.
[28]M. S. Roos, "A technique for the study of acoustic scattering from microparticles," J. Acoust. Soc. Am. **83**, 770–776 (1988).
[29]M. S. Roos, R. E. Apfel, and S. C. Wardlaw, "Application of 30-MHz acoustic scattering to the study of human red blood cells," J. Acoust. Soc. Am. **83**, 1639–1644 (1988).
[30]R. A. Roy and R. E. Apfel, "Mechanical characterization of microparticles by scattered ultrasound," J. Acoust. Soc. Am. **87**, 2332–2341 (1990).
[31]M. L. Oelze, W. D. O'Brien, J. P. Blue, and J. F. Zachary, "Differentiation and characterization of rat mammary fibroadenomas and 4T1 mouse carcinomas using quantitative ultrasound imaging," IEEE Trans. Med. Imag. **23**, 764–771 (2004).
[32]M. L. Oelze and J. F. Zachary, "Examination of cancer in mouse models using high-frequency quantitative ultrasound," Ultrasound Med. Biol. **32**, 1639–1648 (2006).
[33]J. Mamou, A. Coron, M. L. Oelze, E. Saegusa-Beecroft, M. Hata, P. Lee, J. Machi, E. Yanagihara, P. Laugier, and E. J. Feleppa, "Three-dimensional high-frequency backscatter and envelope quantification of cancerous human lymph nodes," Ultrasound Med. Biol. **37**, 345–357 (2011).
[34]A. J. Dapore, M. R. King, J. Harter, S. Sarwate, M. L. Oelze, J. A. Zagzebski, M. N. Do, T. J. Hall, and W. D. O'Brien, "Analysis of human fibroadenomas using three-dimensional impedance maps," IEEE Trans. Med. Imag. **30**, 1206–1213 (2011).
[35]K. A. Wear, "Autocorrelation and cepstral methods for measurement of tibial cortical thickness," IEEE Trans. Ultrason., Ferroelectr. Frequency Control **50**, 655–660 (2003).
[36]T. De'an, W. Weiqi, W. Yuanyuan, and Y. Jianguo, "Estimation of the mean spacing of trabecular bones using autoregression cepstrum," Chin. J. Sci. Instrum. **28**, 17 (2007).
[37]K. A. Wear, R. F. Wagner, M. F. Insana, and T. J. Hall, "Application of autoregressive spectral analysis to cepstral estimation of mean scatterer spacing," IEEE Trans. Ultrason., Ferroelectr., Frequency Control **40**, 50–58 (1993).
[38]J. W. Hunt, A. E. Worthington, A. Xuan, M. C. Kolios, G. J. Czarnota, and M. D. Sherar, "A model based upon pseudo regular spacing of cells combined with the randomisation of the nuclei can explain the significant changes in high-frequency ultrasound signals during apoptosis," Ultrasound Med. Biol. **28**, 217–226 (2002).
[39]A. S. Tunis, G. Czarnota, A. Giles, M. D. Sherar, J. W. Hunt, and M. C. Kolios, "Monitoring structural changes in cells with high-frequency ultrasound signal statistics," Ultrasound Med. Biol. **31**, 1041–1049 (2005).
[40]R. M. Vlad, R. K. Saha, N. M. Alajez, S. Ranieri, G. J. Czarnota, and M. C. Kolios, "An increase in cellular size variance contributes to the increase in ultrasound backscatter during cell death," Ultrasound Med. Biol. **36**, 1546–1558 (2010).
[41]J. McNew, R. Lavarello, and W. D. O'Brien, "Sound scattering from two concentric fluid spheres," J. Acoust. Soc. Am. **125**, 1–4 (2009).
[42]J. C. Bamber and R. J. Dickinson, "Ultrasonic B-scanning: A computer simulation," Phys. Med. Biol. **25**, 463–479 (1980).
[43]C. M. Sehgal and J. F. Greenleaf, "Scattering of ultrasound by tissues," Ultrason. Imag. **6**, 60–80 (1984).
[44]D. R. Foster, M. Arditi, F. S. Foster, M. S. Patterson, and J. W. Hunt, "Computer simulations of speckle in B-scan images," Ultrason. Imag. **5**, 308–330 (1983).
[45]S. H. P. Bly, D. Lee-Chahal, D. R. Foster, M. S. Patterson, F. S. Foster, and J. W. Hunt, "Quantitative contrast measurements in B-mode images comparison between experiment and theory," Ultrasound Med. Biol. **12**, 197–208 (1986).
[46]P. M. Shankar, "A model for ultrasonic scattering from tissues based on the K distribution," Phys. Med. Biol. **40**, 1633 (1995).
[47]R. C. Molthen, P. M. Shankar, and J. M. Reid, "Characterization of ultrasonic B-scans using non-Rayleigh statistics," Ultrasound Med. Biol. **21**, 161–170 (1995).

[48]V. M. Narayanan, P. M. Shankar, and J. M. Reid, "Non-Rayleigh statistics of ultrasonic backscattered signals," IEEE Trans. Ultrason., Ferroelectr., Frequency Control **41**, 845–852 (1994).
[49]V. Dutt and J. F. Greenleaf, "Ultrasound echo envelope analysis using a homodyned K distribution signal model," Ultrason. Imag. **16**, 265−287 (1994).
[50]P. M. Shankar, "A general statistical model for ultrasonic backscattering from tissues," IEEE Trans. Ultrason., Ferroelectr., Frequency Control **47**, 727–736 (2000).
[51]P. M. Shankar, "Ultrasonic tissue characterization using a generalized Nakagami model," IEEE Trans. Ultrason., Ferroelectr., Frequency Control **48**, 1716–1720 (2001).
[52]P.-H. Tsui and C.-C. Chang, "imaging local scatterer concentrations by the Nakagami statistical model," Ultrasound Med. Biol. **33**, 608–619 (2007).
[53]F. L. Lizzi, M. Greenebaum, E. J. Feleppa, M. Elbaum, and D. J. Coleman, "Theoretical framework for spectrum analysis in ultrasonic tissue characterization," J. Acoust. Soc. Am. **73**, 1366–1373 (1983).
[54]F. L. Lizzi, M. Ostromogilsky, E. J. Feleppa, M. C. Rorke, and M. M. Yaremko, "Relationship of ultrasonic spectral parameters to features of tissue microstructure," IEEE Trans. Ultrason., Ferroelectr. Frequency Control **34**, 319–329 (1987).
[55]T. E. Doyle, A. T. Tew, K. H. Warnick, and B. L. Carruth, "Simulation of elastic wave scattering in cells and tissues at the microscopic level," J. Acoust. Soc. Am. **125**, 1751–1767 (2009).
[56]D. Savéry and G. Cloutier, "A point process approach to assess the frequency dependence of ultrasound backscattering by aggregating red blood cells," J. Acoust. Soc. Am. **110**, 3252–3262 (2001).
[57]E. Franceschini and R. Guillermin, "Experimental assessment of four ultrasound scattering models for characterizing concentrated tissue-mimicking phantoms," J. Acoust. Soc. Am. **132**, 3735–3747 (2012).
[58]E. Franceschini, R. Guillermin, F. Tourniaire, S. Roffino, E. Lamy, and J.-F. Landrier, "Structure factor model for understanding the measured backscatter coefficients from concentrated cell pellet biophantoms," J. Acoust. Soc. Am. **135**, 3620–3631 (2014).
[59]E. Franceschini, R. Monchy, and J. Mamou, "Quantitative characterization of tissue microstructure in concentrated cell pellet biophantoms based on the structure factor model," IEEE Trans. Ultrason, Ferroelectr, Frequency Control **63**, 1321–1334 (2016).
[60]M. F. Insana, R. F. Wagner, D. G. Brown, and T. J. Hall, "Describing small-scale structure in random media using pulse-echo ultrasound," J. Acoust. Soc. Am. **87**, 179–192 (1990).
[61]M. Kolios, "Biomedical ultrasound imaging: From 1 to 1000 MHz," Can. Acoust.-Acoust. Can. **37**, 35–43 (2009).
[62]P. Chiarelli, A. Lanatà, and M. Carbone, "Acoustic waves in hydrogels: A bi-phasic model for ultrasound tissue-mimicking phantom," Mater. Sci. Eng. C **29**, 899–907 (2009).
[63]E. Moeendarbary, L. Valon, M. Fritzsche, A. R. Harris, D. A. Moulding, A. J. Thrasher, E. Stride, L. Mahadevan, and G. T. Charras, "The cytoplasm of living cells behaves as a poroelastic material," Nat. Mater. **12**, 253–261 (2013).
[64]P. Chiarelli, B. Vinci, A. Lanatà, C. Lagomarsini, and S. Chiarelli, "Poroelastic longitudinal wave equation for soft living tissues," J. Biorheol. **28**, 29–37 (2014).
[65]M. L. Oelze and W. D. O'Brien, "Application of three scattering models to characterization of solid tumors in mice," Ultrason. Imag. **28**, 83–96 (2006).
[66]R. K. Saha and M. C. Kolios, "Effects of cell spatial organization and size distribution on ultrasound backscattering," IEEE Trans. Ultrason., Ferroelectr. Frequency Control **58**, 2118–2131 (2011).
[67]R. L. Romijn, J. M. Thijssen, and G. W. J. van Beuningen, "Estimation of scatterer size from backscattered ultrasound: A simulation study," IEEE Trans. Ultrason., Ferroelectr., Frequency Control **36**, 593–606 (1989).
[68]R. E. Baddour, M. D. Sherar, J. W. Hunt, G. J. Czarnota, and M. C. Kolios, "High-frequency ultrasound scattering from microspheres and single cells," J. Acoust. Soc. Am. **117**, 934–943 (2005).
[69]O. Falou, R. E. Baddour, G. Nathanael, G. J. Czarnota, J. C. Kumaradas, and M. C. Kolios, "A study of high frequency ultrasound scattering from non-nucleated biological specimens," J. Acoust. Soc. Am. **124**, EL278–EL283 (2008).
[70]O. Falou, M. Rui, A. El Kaffas, J. C. Kumaradas, and M. C. Kolios, "The measurement of ultrasound scattering from individual micron-sized objects and its application in single cell scattering," J. Acoust. Soc. Am. **128**, 894–902 (2010).
[71]A. Han, R. Abuhabsah, R. J. Miller, S. Sarwate, and W. D. O'Brien, "The measurement of ultrasound backscattering from cell pellet biophantoms and tumors *ex vivo*," J. Acoust. Soc. Am. **134**, 686–693 (2013).
[72]A. Han, R. Abuhabsah, J. P. Blue, S. Sarwate, and W. D. O'Brien, "Ultrasonic backscatter coefficient quantitative estimates from high-concentration Chinese hamster ovary cell pellet biophantoms," J. Acoust. Soc. Am. **130**, 4139–4147 (2011).
[73]E. M. Strohm and M. C. Kolios, "Classification of blood cells and tumor cells using label-free ultrasound and photoacoustics," Cytometry, Part A **87**, 741–749 (2015).
[74]V. C. Anderson, "Sound scattering from a fluid sphere," J. Acoust. Soc. Am. **22**, 426–431 (1950).
[75]R. D. Spence and S. Granger, "The scattering of sound from a prolate spheroid," J. Acoust. Soc. Am. **23**, 701–706 (1951).
[76]J. Faran, "Sound scattering by solid cylinders and spheres," J. Acoust. Soc. Am. **23**, 405–418 (1951).
[77]R. Hickling, "Analysis of echoes from a solid elastic sphere in water," J. Acoust. Soc. Am. **34**, 1582–1592 (1962).
[78]A. Silbiger, "Scattering of sound by an elastic prolate spheroid," J. Acoust. Soc. Am. **35**, 564–570 (1963).
[79]R. K. Johnson, "Sound scattering from a fluid sphere revisited," J. Acoust. Soc. Am. **61**, 375–377 (1977).
[80]G. C. Gaunaurd and H. Überall, "Theory of resonant scattering from spherical cavities in elastic and viscoelastic media," J. Acoust. Soc. Am. **63**, 1699–1712 (1978).
[81]F. Jafari, E. L. Madsen, J. A. Zagzebski, and M. M. Goodsitt, "Exact evaluation of an ultrasonic scattering formula for a rigid immovable sphere," Ultrasound Med. Biol. **7**, 293–296 (1981).
[82]A. E. Hay and R. W. Burling, "On sound scattering and attenuation in suspensions, with marine applications," J. Acoust. Soc. Am. **72**, 950–959 (1982).
[83]G. Gaunaurd, "Elastic and acoustic resonance wave scattering," Appl. Mech. Rev. **42**, 143–168 (1989).
[84]G. Giudice, *Developmental Biology of the Sea Urchin Embryo* (Elsevier, Amsterdam, 2012).
[85]F. Lizzi, E. Feleppa, and N. Jaremko, "Liver-tissue characterization by digital spectrum and cepstrum analysis," in *1981 Ultrasonics Symposium*, pp. 575−578.
[86]R. Kuc, K. Haghkerdar, and M. O'Donnell, "Presence of cepstral peak in random reflected ultrasound signals," Ultrason. Imag. **8**, 196–212 (1986).
[87]R. S. Mia, M. H. Loew, K. A. Wear, and R. F. Wagner, "Quantitative estimation of scatterer spacing from backscattered ultrasound signals using the complex cepstrum," in *Information Processing in Medical Imaging*, edited by J. Duncan and G. Gindi (Springer, Berlin, 1997), pp. 513–518.
[88]T. C. Hales, "Historical overview of the Kepler conjecture," in *The Kepler Conjecture*, edited by J. C. Lagarias (Springer, New York, 2011), pp. 65–82.
[89]S. Torquato, T. M. Truskett, and P. G. Debenedetti, "Is random close packing of spheres well defined?," Phys. Rev. Lett. **84**, 2064–2067 (2000).
[90]U. Del Monte and E. G. Caiani, "From Kepler's conjecture and fcc lattice to modelling of crowding in living matter," Ital. J. Anat. Embryol. **118**, 92–104 (2013).
[91]I. Y. Kuo and K. K. Shung, "High frequency ultrasonic backscatter from erythrocyte suspension," IEEE Trans. Biomed. Eng. **41**, 29–34 (1994).
[92]C.-C. Coussios, "The significance of shape and orientation in single-particle weak-scatterer models," J. Acoust. Soc. Am. **112**, 906–915 (2002).
[93]D. Savéry and G. Cloutier, "High-frequency ultrasound backscattering by blood: Analytical and semianalytical models of the erythrocyte cross section," J. Acoust. Soc. Am. **121**, 3963–3971 (2007).
[94]K. V. Mackenzie, "Nine-term equation for sound speed in the oceans," J. Acoust. Soc. Am. **70**, 807–812 (1981).
[95]M. J. Moore, E. M. Strohm, and M. C. Kolios, "Assessment of the nucleus-to-cytoplasmic ratio in MCF-7 cells using ultra-high frequency ultrasound and photoacoustics," Int. J. Thermophys. **37**, 118 (2016).
[96]E. M. Strohm, M. J. Moore, and M. C. Kolios, "Single cell photoacoustic microscopy: A review," IEEE J. Sel. Top. Quantum Electron. **22**, 6801215 (2016).